Journal of Materials Chemistry C

Electric Field- and Light-Responsive Oxadiazole-Bent-Core Polycatenar Liquid Crystals

Journal:	*Journal of Materials Chemistry C*
Manuscript ID	TC-ART-11-2023-004349.R1
Article Type:	Paper
Date Submitted by the Author:	15-Dec-2023
Complete List of Authors:	Alaasar, Mohamed; Martin-Luther-University- Halle-Wittenberg, Institute of Chemistry; Cairo University, Faculty of Science Darweesh, Ahmed; Cairo University-Faculty of Science, Chemistry Giza, Egypt, Chemistry Cao, Yu; Xi'an Jiaotong University, ; Iakoubovskii, Konstantin; National Institute for Materials Science, Masafumi, Yoshio; National Institute for Materials Science, Functional Materials; Hokkaido University Graduate School of Chemical Sciences and Engineering,

Electric Field- and Light-Responsive Oxadiazole-Bent-Core Polycatenar Liquid Crystals

Mohamed Alaasar,*[a] Ahmed F. Darweesh,[b] Yu Cao,[c] Konstantin Iakoubovskii,*[d] Masafumi Yoshio[d,e]

[a]Institute of Chemistry, Martin Luther University Halle-Wittenberg, 06120 Halle, Germany
[b]Department of Chemistry, Faculty of Science, Cairo University, 12613 Giza, Egypt
[c]Shaanxi International Research Center for Soft Matter, State Key Laboratory for Mechanical Behavior of Materials, Xi'an Jiaotong University, Xi'an 710049, P. R. China
[d]Research Center for Macromolecules & Biomaterials, National Institute for Materials Science, 1-2-1 Sengen, Tsukuba, Ibaraki 305-0047, Japan
[e]Japan Science and Technology Agency, PRESTO, 4-1-8 Honcho, Kawaguchi, Saitama, 332-0012, Japan

Abstract

Alkyl chain engineering of polycatenar liquid crystals (LCs), which consist of a rigid aromatic core with flexible chains at both ends, serves as an effective method for controlling their self-assembled nanostructures. Incorporating stimuli-responsive molecular units into the design of polycatenars represents a promising strategy for developing novel functional LC materials. In this study, we present the design and synthesis of new oxadiazole-based bent-core tetracatenar LCs with alkoxy azobenzene terminals. These compounds form 3D bicontinuous cubic (Cub_{bi}) or columnar phases depending on the length of the terminal chains. The shortest homologue displays a Cub_{bi} phase of the double gyroid type ($Cub_{bi}/Ia\bar{3}d$) and a triple-network phase with $I23$ space group ($Cub_{bi}/I23$). Longer homologues form a hexagonal columnar LC phase. This columnar phase could be aligned by cooling a molten sample under applied electric field, and the alignment was attributed to dielectric polarization induced by the oxadiazole ring. Furthermore, the incorporation of fluorinated azobenzene facilitated orientation switching from a random to aligned state within the columnar LC phases. Using UV irradiation, we successfully modified the LC phase structure via the reversible *trans-to-cis* photoisomerization of the azobenzene units. These findings underscore the potential applications of the reported materials in information-storage devices.

Keywords: Bent-core liquid crystals; polycatenars; oxadiazole; ferroelectricity; azobenzene; columnar phases

1. Introduction

The search for new materials that can be used for optoelectronic and electronic devices, such as field-effect transistors, light-emitting diodes and solar cells, is a hot topic that attracts a wide range of materials scientists.[1,2,3,4,5] Organic materials for such applications have several advantages compared to inorganic ones, because they are relatively abundant, non-toxic, inexpensive and can be easily modified.[3,6] Organic liquid crystals (LCs) represent one important class of such promising materials in different renewable technological applications.[7] LCs are characterized by their ability to respond to external stimuli, such as electric field, resulting in tailor-made nanostructures. Photo-responsive LCs derived from azobenzene-based materials exhibit reversible *trans-to-cis* photoisomerization. They have been studied for several decades,[8,9] and still attract researchers as they can exhibit macroscopic changes upon atomic-scale modifications.[10-19] Combining semiconductors with azobenzene and using strain engineering as a result of photoisomerization holds promise for electronic device applications.[20] Columnar LCs can have high and anisotropic mobility of charge carriers, which is required for electronic applications.[21-24] This is because in a columnar phase, each column provides a one-dimensional path for charge transport through its central part, which is composed of rigid molecular cores. Meanwhile, the flexible terminal chains of the molecules isolate those columns as a result of the nano-segregation of incompatible molecular subunits.[25,26] Various molecular structures exhibiting columnar LC phases have been tested for optoelectronic applications including organic light emitting diodes [27,28,29,30] and field-transistors.[31,32]

A large variety of unconventional molecular designs that differ from traditional calamitic or discotic LCs systems have been reported.[33] Polycatenar LCs having multiple flexible terminal chains are an important class of such unconventional structures.[33] Recently, it was found that polycatenar LCs with nonsymmetrical terminal chains with respect to the rod-like aromatic core could exhibit interesting nano-structured LC phases. Those include bicontinuous cubic (Cub_{bi}) phases with $I23$ symmetry, which exhibit a mirror symmetry and were initially assigned as $Im\bar{3}m$,[34] as well as an achiral version with $Ia\bar{3}d$ space group.[35] These Cub_{bi} phases are composed of three-dimensional networks with three-way junctions, where the double gyroid ($Cub_{bi}/Ia\bar{3}d$) contains two of such networks with opposite chiralities, while three helical networks are present in the $Cub_{bi}/I23$ phase. Chirality was even observed in the isotropic liquid networks of these molecules.[36] Different aromatic core units were used to design such nonsymmetric polycatenars, including π-conjugated 5,5'-diphenyl-2,2'-

bithiophene,[37-40] π-conjugated [1]benzothieno[3,2-b]benzothiophene [41,42] and azobenzene moiety.[43-47] Only in a few studies nonsymmetric hockey-stick polycatenars were constructed using 2,5-disbstituted thiophene [48] or 4-cyanoresorcinol as bent-core units.[49,50] None of these materials had polar LC phases, which are usually exhibited by bent-core mesogens; instead, non-polar lamellar smectic A, Cub_{bi} or columnar phases were observed. A promising unit for designing bent-core (banana) LCs is the ~135° bent 1,3,4-oxadiazole core, which can form biaxial nematic,[51-55] polar and chiral nematic and smectic phases.[56-64] It has also been used for designing star-shaped fluorescent columnar LC phases.[65-70]

In this work, we have combined azobenzene and 1,3,4-oxadiazole to design and synthesize hockey-stick nonsymmetric polycatenars (**Scheme 1**). These molecules have the same mesogenic core terminated with three hexadecyloxy chains at one end and a variable alkoxy chain at the other end. The corresponding LCs show a transition from two different types of Cub_{bi} to columnar phases, depending on the terminal chain length attached to the azobenzene-based core. The incorporation of oxadiazole into the molecular core facilitated the alignment of LC columns by applied electric field during cooling from the isotropic phase, owing to the polarization induced by the oxadiazole ring. Additional fluorination of the aromatic core induced ferroelectricity in the columnar LC phase. The presence of azobenzene in the core allowed us to exploit its *trans-to-cis* photoisomerization, which resulted in reversible structural changes in the LC phase. All these mechanisms, combined in one molecule, lead to a versatile tunable nanostructure with potential optoelectronic applications.

2. Results and discussion

2.1. Synthesis

The synthesis of the oxadiazole-derived polycatenars (**A*n***, **A12F$_3$** and **A12F$_{23}$**) is illustrated in **Scheme 1** and is detailed in the Supporting Information. It started with the esterification of commercially available 4-benzyloxybenzoic acid (**1**) and pentafluorophenol (**2**), followed by reaction of the obtained intermediate **3** with 4-hydroxybenzoic acid hydrazide (**4**) to give compound **5**. Compound **5** was cyclized using thionyl chloride ($SOCl_2$), resulting in the 1,3,4-oxadiazole heterocyclic intermediate **6** with a benzyl protecting group.[71] The highly reactive acyl chloride of 3,4,5-trihexadeclyoxybenzoic acid (**7**),[72] generated using $SOCl_2$ and a catalytic amount of *N,N*-dimethylformamide (DMF), was used in acylation reaction of the phenol **6** to obtain the protected compound **8**, which was unprotected via hydrogenation in

presence of palladium on activated carbon. At the last synthesis stage, another acylation reaction was performed between the acyl chlorides of the different azobenzene-based benzoic acid derivatives **10*n*** [45] with the phenol **9** to yield the final polycatenars. The crude materials were purified by column chromatography using $CHCl_3$/ethylacetate (4:1) as an eluent, followed by recrystallization from chloroform/ethanol (77−90% yield). The materials were characterized by ^1H and ^{13}C nuclear magnetic resonance and elemental analysis (see Supplemental Information). All data agreed with the proposed molecular structures of the targeted compounds.

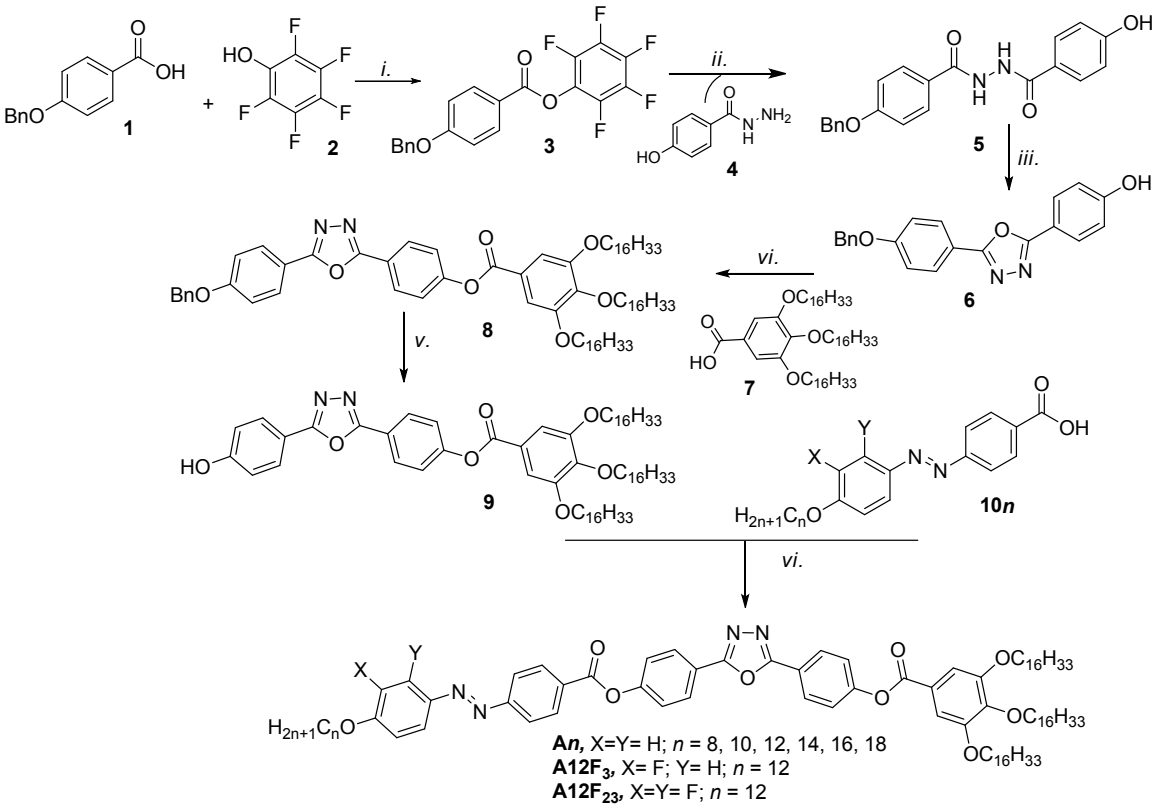

Scheme 1. Synthesis of the target hockey-stick polycatenars **A*n***, **A12F$_3$** and **A12F$_{23}$**. Reagents and conditions: *i*. *N,N*'-dicyclohexylcarbodiimide, dichloromethane (DCM) and 4-dimethylaminopyridine, stirring at room temperature (RT), 72 h; *ii*. DMF, stirring at RT, 48 h; *iii*. $SOCl_2$, dry pyridine, reflux under argon atmosphere, 4 h; *vi*. $SOCl_2$, dry pyridine, triethylamine, DCM, reflux under argon atmosphere, 4 h; *v*. Pd/C 10%, H_2, dry tetrahydrofuran, stirring at RT, 24 h.

2.2. Characterization methods

Polarized optical micrographs (POMs) were acquired under the crossed Nicol's condition. Differential scanning calorimetry (DSC) traces were recorded with DSC-7 and DSC-8000 Perkin Elmer setups, in Ar flow, at a heating or cooling rate of 10 K min^{-1}.

Small-angle X-ray scattering (SAXS) experiments were conducted at the BL16B1 beamline of the Shanghai Synchrotron Radiation Facility (SSRF). For powder SAXS, samples were filled into evacuated 1 mm diameter capillaries. Data calibration was conducted using silver borohydride and a series of *n*-alkanes.

The conversion of 2D data to 1D plots was carried out using the Gauss equation implemented in the Irena and Nika macro packages within Igor64 software. After indexing and integrating SAXS peaks, electron density maps were reconstructed via Fourier transform as

$$\rho(x,y,z) = \sum_{hkl} \sqrt{I(hkl)} \exp\left[2\pi i(hx + ky + lz) + i\phi_{hkl}\right]$$

For centrosymmetric structures with $\rho(x,y,z) = \rho(\bar{x},\bar{y},\bar{z})$, the phase ϕ_{hkl} is either 0 or π, and hence all possible phase permutations can be tried. The best combination is decided by the physical merit of reconstructed electron density map and by other details, like the volume ratio of aromatic/aliphatic region and electron density distribution histogram.

Samples for electro-optical measurements were prepared by filling commercial cells from EHC, Japan. The cells consisted of two 0.7-mm-thick glass plates coated with 20 nm of indium tin oxide. Epoxy spacers separated them by a distance of 4 μm (cells with a spacing of 2 and 9 were also tried, but the results were inferior, and hence were omitted). The overlapping area between the top and bottom electrodes was 4×4 mm. Cells were filled in vacuum, in darkness, at a temperature 5 °C above the isotropic point, within 1 hour. A small amount of powdered material was placed on the edge of a cell, where it melted, and was driven into the cell by capillary force.

Second harmonic generation (SHG) measurements were carried out with a pulsed Q-switched Nd-doped yttrium aluminium garnet laser (Nd:YAG, Continuum Minilite II, Amplitude, Japan; 1064 nm, 6 ns, ~0.1 mJ) and a SEC2020 spectrometer equipped with a 1D Si array detector (ALS, Japan). This spectrometer was also used for optical absorption measurements.

2.3. Thermal behavior: DSC and POM

Combined POM and DSC results for **A*n*** compounds are summarized in **Table 1** and **Figures S9-S10**.

Table 1. Phase transitions of compounds **A*n***, **A12F$_3$** and **A12F$_{23}$**.[a]

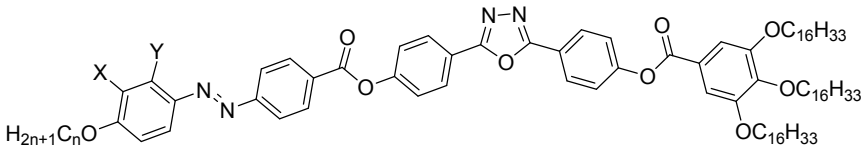

Name	X	Y	Phase transitions T/°C [ΔH/kJ mol^{-1}]
A8	H	H	**H:** Cr 103 [51.9] Mix 114 [< 0.1] Cub$_{bi}$/*Ia*$\bar{3}$*d* 126 [1.3] Iso **C:** Iso 112 [-0.7] Col$_{hex}$ 111 [< 0.1] Cub$_{bi}$/*Ia*$\bar{3}$*d* 101 [1.1] Cub$_{bi}$/*I*23$^{[*]}$ 80 [-62.3] Cr
A10	H	H	**H:** Cr 104 [73.2] Col$_{hex}$ 144 [1.3] Iso **C:** Iso 141 [-1.3] Col$_{hex}$ 76 [-71.5] Cr
A12	H	H	**H:** Cr 100 [83.3] Col$_{hex}$ 135 [1.3] Iso **C:** Iso 131 [-1.3] Col$_{hex}$ 71 [-81.7] Cr
A14	H	H	**H:** Cr 101 [55.5] Col$_{hex}$ 137 [1.5] Iso **C:** Iso 133 [-1.4] Col$_{hex}$ 76 [-58.8] Cr
A16	H	H	**H:** Cr 84 [76.4] Col$_{hex}$ 139 [1.8] Iso **C:** Iso 135 [-1.5] Col$_{hex}$ 54 [-88.3] Cr
A18	H	H	**H:** Cr 85 [136.8] Col$_{hex}$ 135 [2.0] Iso **C:** Iso 132 [-2.2] Col$_{hex}$ 56 [-90.0] Cr
A12F$_3$	F	H	**H:** Cr 107 [58.1] Col$_{hex}$ 142 [1.6] Iso **C:** Iso 139 [-1.6] Col$_{hex}$ 65 [-66.8] Cr
A12F$_{23}$	F	F	**H:** Cr$^{[*]}$ 115 [51.9] Col$_{hex}$ 121 [0.8] Iso **C:** Iso 118 [-0.9] Col$_{hex}$ 85 [-47.7] Cr$^{[*]}$

[a]Peak temperatures as determined by DSC upon 2nd heating (**H:**) and 2nd cooling (**C:**) with a rate of 10 K min^{-1}. Abbreviations: Cr = crystalline solid phase; Iso = isotropic liquid phase; Col$_{hex}$ = hexagonal columnar phase; Cub$_{bi}$/*Ia*$\bar{3}$*d* = achiral bicontinuous cubic phase with *Ia*$\bar{3}$*d* space group; Cub$_{bi}$/*I*23$^{[*]}$ = chiral bicontinuous cubic phase with *I*23 space group; Cr$^{[*]}$ = chiral crystalline phase; Mix = a mixture of Cub$_{bi}$/*Ia*$\bar{3}$*d*, Cub$_{bi}$/*I*23$^{[*]}$ and crystalline solid phase.

Initial phase characterization was performed using POM, both on heating and cooling. The phase behavior of the shortest homologue with n = 8 (**A8**) is different from other **A*n*** members, and therefore it is discussed in detail. Upon cooling of **A8** from the isotropic liquid state, a birefringent texture is observed under crossed polarizers (**Figure S9a**). This fan-shaped texture is fluid and shearable, which is typical for a columnar LC phase (Col). It exists in a narrow temperature range of ~1 K and is replaced by a highly viscous and completely dark phase (Fig. S9b), which persists until crystallization at ~80 °C. When one of the polarizers is slightly rotated either clockwise or anticlockwise, no dark and bright domains could be detected, suggesting the presence of a nanostructured double gyroid (Cub$_{bi}$/*Ia*$\bar{3}$*d*).

On heating the birefringent crystalline state of **A8** only the isotropic phase could be observed, indicating that the columnar phase is metastable. This observation agrees with the DSC heating scan (see **Figure S10**), where only one transition around 126 °C is observed besides the melting peak. In the DSC cooling scan, the isotropic-columnar transition could be detected at ~112 °C, followed by another transition at ~ 101 °C. For this transition, no structural

change in the isotropic texture could be detected by POM, no matter the cell thickness and cooling rate.

SAXS measurements revealed that the 101 °C transition leads to the second nanostructured Cub_{bi} phase with *I*23 space group (Cub_{bi}/*I*23), which usually do display chiral domains.[36-39,45] This represents the second case when macroscopic conglomerates were not detected in the *I*23 phase of a polycatenar material, following our recent report on linear polycatenars.[46] Owing to the spontaneous formation of two cubic phases (Cub_{bi}/$Ia\bar{3}d$ and Cub_{bi}/*I*23), the cubic domains are small and random. This leads to the absence of chiral conglomerates that could be detected by POM.

Continuous heating and cooling scans were preformed to confirm the **A8** phases. Two cubic phases were indexed, and the electron density map was reconstructed as shown in **Figure 1.** At 102 °C upon heating, a complex scattering pattern was observed and indexed as a mixture of two cubic LC and one crystal phases (Fig. S12a). The (211) Cub_{bi}/$Ia\bar{3}d$ peak becomes stronger, and both cubic phases coexist until 114 °C, when the Cub_{bi}/$Ia\bar{3}d$ phase remains (Figure 1a). The isotropic state is observed at 126 °C. The reconstructed electron density map in Figure 1c suggests that the Cub_{bi}/$Ia\bar{3}d$ phase is a *meso*-structure comprising two interwoven continuous networks with opposite handedness, which are conjugated by three-way junctions. The aromatic cores construct networks with high electron density. Flexible alkyl chains fill the rest of the lattice. Due to the nonsymmetric and twisted nature, the molecules first combine into molecular rafts that lie perpendicularly to the networks. Then the rafts twist along the networks, forming molecular helices of opposite handedness and cancelling the chirality (Figure 1e). Such molecular twists would also cancel the mismatch at the three-way junctions, and thus should be energetically favored. The lattice parameter of this cubic phase is 12.83 nm, and the number of molecules per unit cell is ~900. Considering the average spacing between molecules as 0.45 nm and the network period $L_{net} = 8.485a_{Ia3d} \approx 109$ nm,[46] there are ~109/0.45 ≈240 molecular rafts in the lattice with about 900/240 ~ 3.7 molecules per raft as shown in Figure 1e. Given the fixed dihedral angle between neighboring junctions of $2\times\text{asin}(1/\sqrt{3}) = 70.5°$,[34] we can estimate the twist angle between rafts as $70.5°/(0.354a_{cub}/0.45\text{nm}) \approx 7°$.[34]

Upon cooling from isotropic phase, a hexagonal columnar phase was first observed with a lattice parameter of 5.82 nm. This columnar phase swiftly converts into an *I*23 cubic phase (Figure 1b). Such a non-centrosymmetric space group provides the opportunity for supramolecular chirality while retaining the local chemical environment (three-way junctions).

In this phase, instead of a *meso*-structure, three networks were formed with molecular helices aligned as shown in Figure 1d, f. In this arrangement, the chirality from molecular helices is not cancelled by the networks as in the $Ia\bar{3}d$ phase. The unit cell of this phase has a length of 20.24 nm and contains ~3525 molecules. The corresponding network has a length $L_{net} \approx 20.68a_{I23} \approx 420$ nm and contains ~420/0.45 ≈ 930 molecular rafts with ~3.8 molecules per raft, similar to the $Ia\bar{3}d$ phase. The twist angle between neighboring rafts is $90°/(0.290a_{cub}/0.45\text{nm}) \sim 6.9°$.[46] It is slightly smaller compared to the $Ia\bar{3}d$ phase because of the lower temperature range for the *I*23 phase. The coherence length of the *I*23 phase was estimated as 190 nm from the width of SAXS peaks. Such a small value explains the absence of chiral conglomerates in POM images. A more comprehensive overview of phases is provided in Section 7 of Supporting Information.

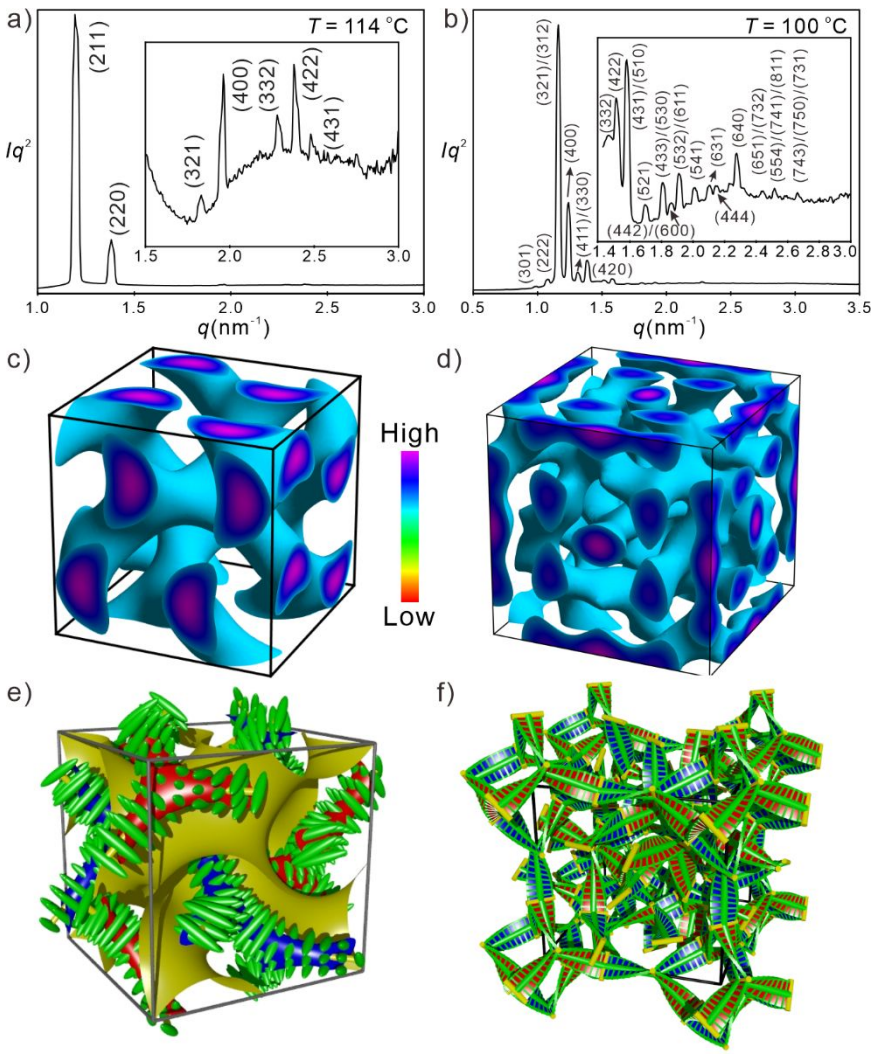

Figure 1. SAXS data of **A8:** a) $Cub_{bi}/Ia\bar{3}d$ phase observed at 114 °C upon heating and b) $Cub_{bi}/I23$ phase at 100 °C upon cooling. Electron density maps of the c) $Cub_{bi}/Ia\bar{3}d$ and d) $Cub_{bi}/I23$ phases; high electron density is in purple and low electron density (red) is omitted for clarity. Geometric model of the e) $Cub_{bi}/Ia\bar{3}d$ and f) $Cub_{bi}/I23$

phases; molecular rafts are represented by green rods. (e) and (f) were reproduced with permission of Wiley-VCH (copyright 2014) (ref 30) and Royal Society of Chemistry (copyright 2020) (ref. 32), respectively.

A*n* compounds with $n \geq 10$ exhibited only columnar LC phases, and their temperature ranges (~35–55 K depending on *n*, see **Figures S9c,d** for examples) are much wider compared to **A8**. The Col-Iso transition was observed in DSC heating and cooling cycles (see **Table 1** and **Figure S10b**). Its enthalpy increases with *n* from 1.3 to 2.0 kJ mol^{-1}. The melting temperatures are almost the same for **A10-A14**; they decrease for **A16** and **A18**, resulting in wider ranges of columnar phase in the last two cases.

SAXS investigations were performed to elucidate the structure of Col phases. All compounds except **A8** form a single hexagonal phase, as evidenced by the characteristic ratio of SAXS peaks positions of $1{:}\sqrt{3}{:}\sqrt{4}{:}\sqrt{7}$ (see Figure S13a). Taking **A14** as an example, the lattice parameter of the hexagonal phase is 5.64 nm. The reconstructed electron density map suggests a highly averaged columnar phase as shown in Figure S13b. Since there is only one column in each lattice, the number of molecules per raft, n_{raft}, can be estimated as 5. Comparing all compounds **A*n*** at (almost) the same temperature, n_{raft} decreases with ***n*** (Figure S14). When alkyl chain size increases, the peripheral volume expands while the size of aromatic region remains constant. Thus, n_{raft} decreases for **A10-A14**. For **A16** and **A18**, the core/peripheral size ratio becomes stable, which correlates with the wider temperature range of hexagonal columnar phase.

Its symmetry was decided as *p6mm* (Col_{hex}/*p6mm*) based on inobservation of SHG signal. Note that SHG was well detected for non-centrosymmetric phases under the same experimental conditions.

The formation of Col_{hex} for all longer derivatives with $n \geq 10$ could be understood based on the increased aromatic-aliphatic inter-material dividing surface curvature because of the alkyl chain elongation. This results in a transition from infinite continuous networks (Cub_{bi} phases) with minimal surface in **A8** to fully enclosed columns in case of Col_{hex} of **A10–A18**.

2.4. Polarization by electric field

We have introduced oxadiazole to the core of the studied molecules with the aim to polarize them by applied electric field, relying on the relatively large dipole moment of oxadiazole (3.04 D [73]). Such polarization was successfully achieved for columnar phases, as demonstrated on example of **A12** in **Figure 2**; it was not detected in the cubic phases of compound **A8**. In particular, application of a modest DC electric field of 5 V μm^{-1}, normal to the sandwich-type

sample, darkened the area between the electrodes (**Fig. 2a**), while the areas outside the electrodes retained their birefringence (**Fig. 2b**).

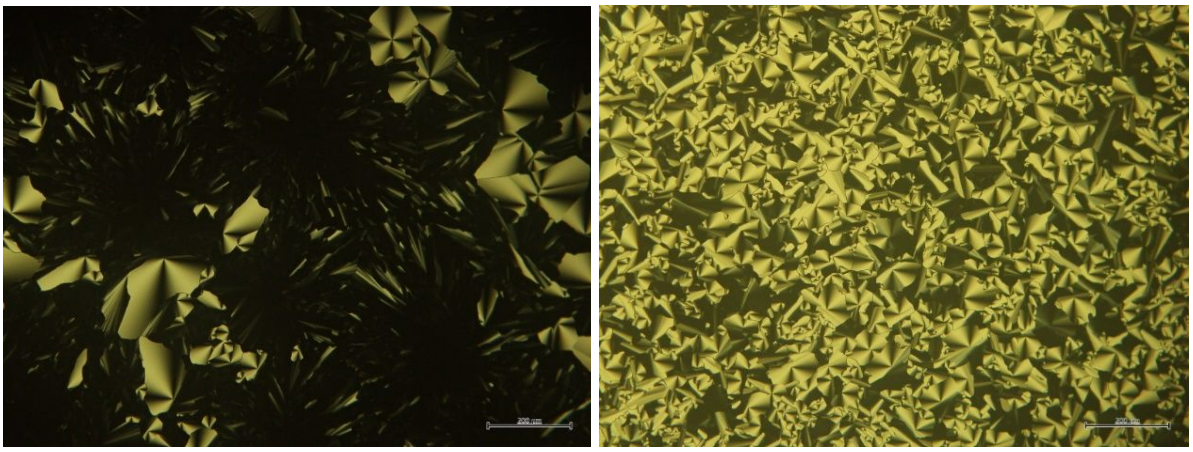

Figure 2. Columnar phase of **A12** viewed between crossed polarizers at 118 °C, after cooling from the temperature above the isotropic point under 5 V μm^{-1} electric field: a) inside, b) outside the electrode area. Scale bar is 200 μm.

To achieve this alignment, it was necessary to heat the sample above the isotropic transition temperature. Alignment was not observed at lower temperatures, presumably due to the high rigidity of the oxadiazole unit in the molecular core. To overcome this problem, we have created a polar and easily rotatable fluorobenzene group in the LC core. The resulting compounds **A12F$_3$** and **A12F$_{23}$** (**Table 1**) have the same chain length as **A12** and different F substitution patterns. In **A12F$_3$**, a fluorine atom is introduced at an ortho position with respect to the terminal alkoxy chain, while in **A12F$_{23}$**, F substitutes for hydrogens both in the ortho and meta positions. Comparing these two materials with their nonfluorinated analogue **A12**, it could be seen from Table 1 that in both cases the melting temperature is increased, presumably due to enhanced core-core interactions. Therefore, the melting temperature of **A12F$_{23}$** (115 °C) is higher than that of the monofluorinated derivative **A12F$_3$** (107 °C). Both derivatives show the same Col_{hex} phase observed in **A12**, as confirmed by POM and SAXS (see **Table 1** and Supplemental Information). Another interesting feature of fluorine is observed for **A12F$_{23}$**, where chirality could be induced in its crystalline state as confirmed from POM investigations (Fig. S9e,f). This could be explained by the increased twisting of the columns at the moment of starting crystallization leading to the observation of chiral domains. These domains are stable and disappear only on reheating the sample at the transition to the Col_{hex} phase.

Fluorination decreases the LC lattice parameter *a* from 5.70 nm in **A12**, to 5.50 nm in **A12F$_3$**, and 5.38 nm in **A12F$_{23}$** (see **Tables S5, S9** and **S10**) This decrease can be explained by the strong inductive effect of fluorine, which reduces the electron density of the core and

increases the core-core interaction. Nevertheless, these high-temperature (~110 °C) *a* values are similar. A different trend was observed for the crystal phases at room temperature, namely *a* = 3.4 nm for **A12**, *a* = 3.2 nm for **A12F$_3$**, and a much larger value *a* = 4.9 nm for **A12F$_{23}$**. Furthermore, SHG signal was detected for **A12F$_3$** (see **Figure S13c** for its spectrum), but not for **A12** or **A12F$_3$**. These results confirm the presence of a chiral crystal phase for **A12F$_{23}$**, which was identified by POM (see **Figure S9e,f**). This phase lacks an inversion center and hence exhibits SHG. Meanwhile, **A12** and **A12F$_3$** crystallize in a centrosymmetric lattice, which has a different *a* value, and lacks the SHG signal.

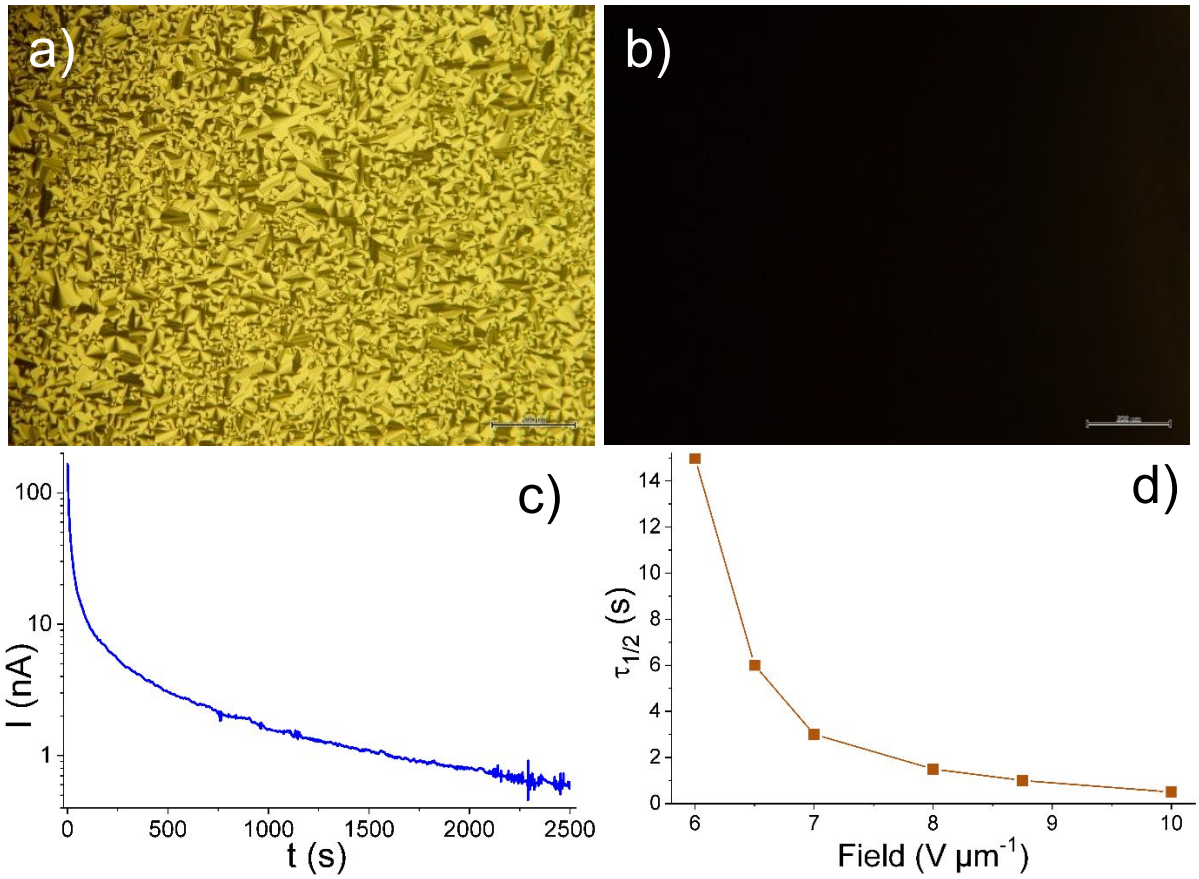

Figure 3. Columnar phase of **A12F$_{23}$** viewed between crossed polarizers at 118 °C: a) at zero field, b) 1 minute after applying an electric field of 5 V µm^{-1} (scale bar 200 µm), c) relaxation of dark current after switching off the field; d) "switching time" required to reduce the birefringence signal intensity twice, plotted vs. applied field.

After fluorination of **A12**, we have achieved switching of birefringence not only in the isotropic, but also in the columnar LC phase, as demonstrated on example of **A12F$_{23}$** in **Figure 3**. Application of the same DC electric field of 5 V µm^{-1} to the LC phase completely erased the birefringence within one minute (**Figure 3a,b**). A current of ~5 µA was measured under the field; it quickly dropped by ~1000 times, and yet remained at the 1 nA level for almost one hour after switching off the field, revealing residual ferroelectric polarization (**Fig. 3c**). The "switching time", which we arbitrarily defined as the time to reduce the birefringence intensity

twice, was relatively slow at 5 V μm^{-1}, but it could be reduced to under one second by doubling the field (see **Fig. 3d**).

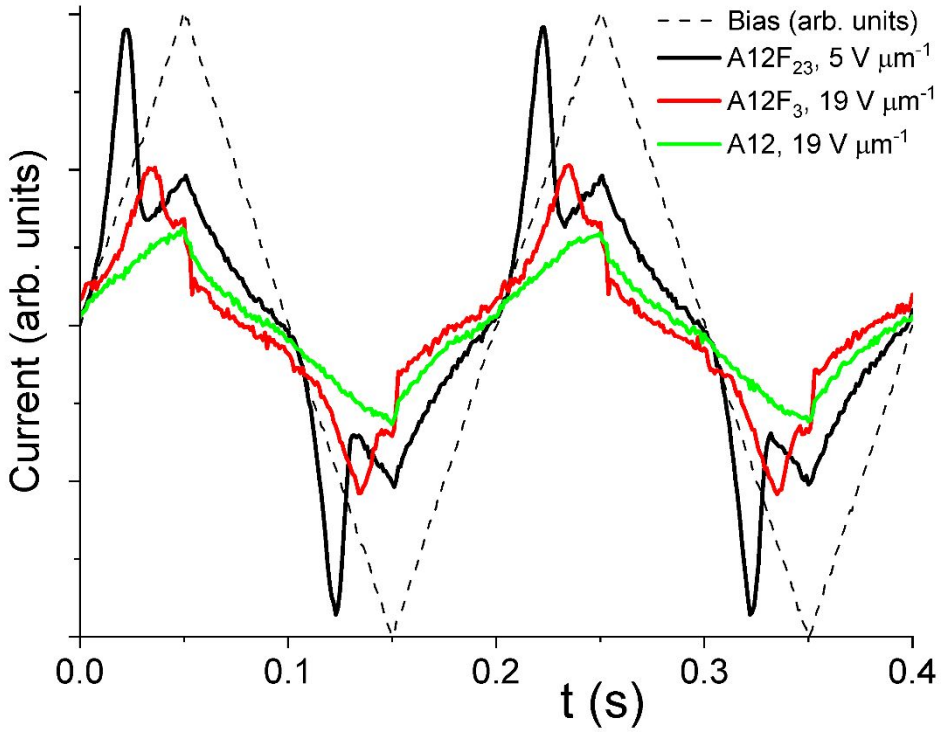

Figure 4. AC current induced at 118 °C by triangular voltage pulses with an amplitude of ±5 V μm^{-1} for **A12F$_{23}$** and ±19 V μm^{-1} for **A12** and **A12F$_3$**. The corresponding maximum polarization is 2.5 μC cm^{-2} for **A12F$_{23}$**.

We have characterized dielectric polarization in **A12**, **A12F$_3$** and **A12F$_{23}$** compounds not only under DC, but also under AC bias. **Figure 4** summarizes a standard poling experiment, in which a triangular voltage was applied at a frequency of 5 Hz, and the switching current was recorded as a voltage drop over a 10 kΩ resistor. A clear polarization peak was observed for **A12F$_{23}$** at a field of 2-5 V μm^{-1}, but not for other materials. The polarization peak appeared in **A12F$_3$**, but only at a bias exceeding 18 V μm^{-1}, and it was not observed in **A12** even near the breakdown field of ~20 V μm^{-1}. These results confirm that the fluorobenzene fragments are responsible for the dielectric (or ferroelectric as in **A12F$_{23}$**) switching, and the lower threshold field in **A12F$_{23}$** can be naturally explained by the higher dipole moment of the difluorobenzene compared to fluorobenzene (2.46 vs. 1.60 D [74]).

We have performed a standard impedance analysis for the AC switching behavior in **A12F$_{23}$** and summarized the results in the Supplemental Information. They reveal that application of a 0.175 V μm^{-1} bias (which is the limit of our impedance analyzer) increased the dielectric constant of the columnar phase from 7 to 10 at 0.1 MHz, and that this change originated from the bulk rather than interfacial layers.

2.5. Photochromism

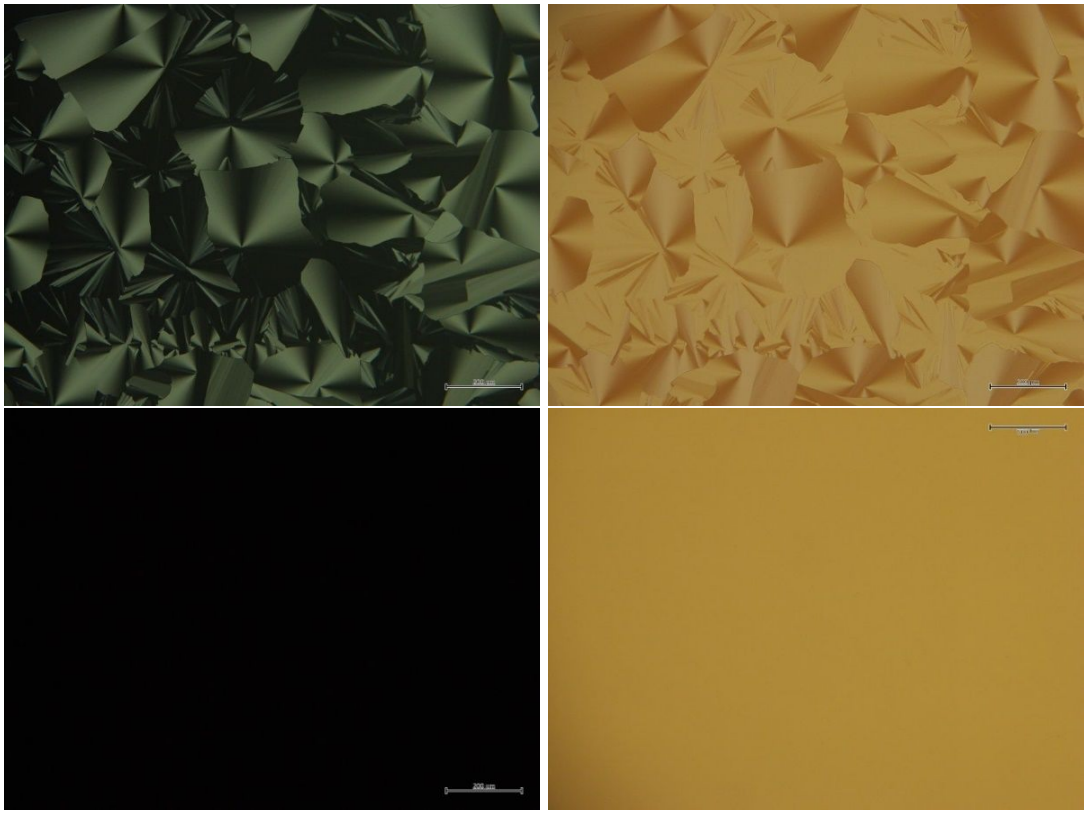

Figure 5. Columnar phase of **A12** viewed at 90 °C upon cooling between crossed polarizers (left) and parallel polarizers (right), before (top row) and after irradiation with 350 nm light (bottom row). Scale bar is 200 μm.

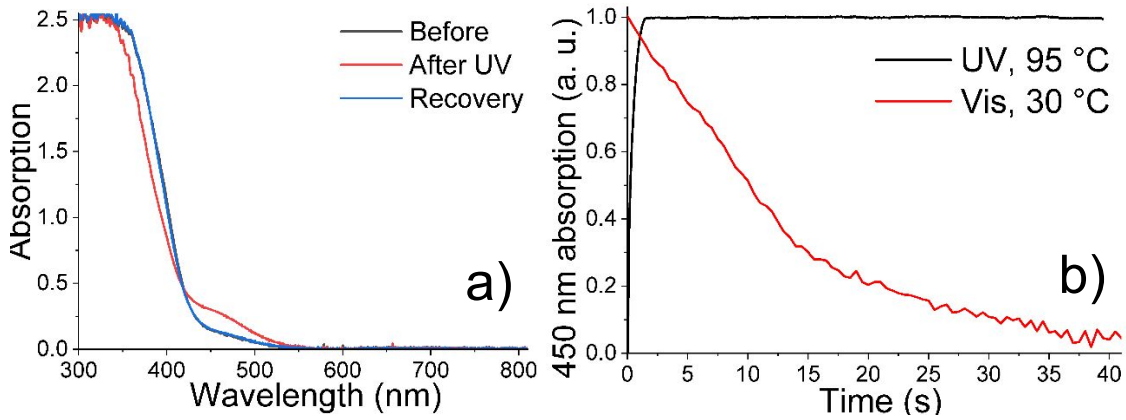

Figure 6. a) Optical absorption spectra from **A12**: initial; right after the sample was irradiated with 350 nm light at 90 °C and cooled under UV light to 30 °C; and 12 hours after keeping the sample at 30 °C in the dark. b) Normalized kinetics of 450 nm absorption: increase under 350 nm light at 90 °C, and relaxation under visible illumination at 30 °C.

The core of all the studied molecules contains azobenzene, which is known to undergo *cis-to-trans* transition under UV illumination. This transition has been widely studied in azobenzene-based LCs in a solution, where the intermolecular interactions are weak and do not

hinder the photoisomerization. Meanwhile, photoisomerization studies in the solids are rare.[17,18,19]

Here we characterize photochromism in the LC state.[16,43,45,75,76] When columnar **A*n*** LCs were irradiated by 350 nm light of 40 mW cm^{-2} intensity, their domain texture and birefringence disappeared within one second, as demonstrated in **Figure 5** on example of **A12**; such changes were not observed for the cubic-phase compound **A8**, either by optical microscopy or by SAXS. The birefringence would recover within one minute after switching off the light. The corresponding optical absorption spectra (**Figure 6a**) showed a reduction in the 370 nm band and an increase in the 450 nm absorption after UV illumination. The absorption completely recovered after storing the sample at ambient conditions in the dark overnight, or after illuminating the sample for one minute with bandpass-filtered visible light (490-760 nm, 100 mW cm^{-2}). Although the optical absorption could be recovered at room temperature, the restoration of domain texture and birefringence required remelting the sample.

The disappearance of LC domains under UV illumination reveals amorphization, which was confirmed by SAXS and DSC measurements (see **Figure S17**). These results can be rationalized as follows: UV illumination changed the molecular shape via isomerization of the azobenzene groups. This modification altered the optical absorption spectra and resulted in semi-permanent amorphization. The optical spectra could be restored by one-minute irradiation with visible light. This phenomenon can be utilized in optical information-storage devices.

3. Summary and conclusions

We have reported on the design and synthesis of new functional light-responsive LCs. We demonstrated that incorporating the stimuli-responsive oxadiazole and azobenzene units into the molecular structure of polycatenars is a promising strategy for producing novel functional LC materials. Depending on the terminal chain length, different types of LC phases were observed, ranging from 3D bicontinuous cubic (Cub_{bi}) to columnar phases. The Cub_{bi} phases are of either double-gyroid (Cub_{bi}/*Ia*$\bar{3}$*d*) or triple-network type (Cub_{bi}/*I*23). According to SAXS investigations, the columnar phases have hexagonal *p*6mm symmetry. Alignment of columnar LC phases was achieved by cooling a molten sample under an applied electric field, and was mediated by the polarization of the oxadiazole ring. Aromatic core fluorination was used as an efficient tool to induce ferroelectricity in the columnar phases. Moreover, through UV irradiation, we were able to modify the LC phase structure via the reversible *trans-to-cis* photoisomerization of the azobenzene units. These findings provide a new concept for

nanostructured functional materials for potential applications such as optical information-storage devices.

Acknowledgements

M. Alaasar acknowledges the German Research Foundation (DFG) for the financial support (AL2378/1-2, 424355983). A. F. Darweesh acknowledges the support by the Alexander von Humboldt Foundation for the research fellowship at Martin Luther University Halle-Wittenberg, Germany.

M. Yoshio acknowledges financial support from Japan Science and Technology Agency (no. JPMJPR23QB) and Iketani Science and Technology Foundation (no. 0351202-A).

Y. Cao acknowledges the National Natural Science Foundation of China (No. 12204369), Science and Technology Agency of Shaanxi Province (2023-YBGY-459), China Postdoctoral Science Foundation (2022M712551, 2023T160505) and beamline BL16B1 at Shanghai Synchrotron Radiation Facility for providing beamtimes.

4. References

1 B. Roy, N. De and K. C. Majumdar, *Chem. - A Eur. J.*, 2012, **18**, 14560–14588.

2 S. Laschat, A. Baro, N. Steinke, F. Giesselmann, C. Hägele, G. Scalia, R. Judele, E. Kapatsina, S. Sauer, A. Schreivogel and M. Tosoni, *Angew. Chemie - Int. Ed.*, 2007, **46**, 4832–4887.

3 U. H. F. Bunz and J. Freudenberg, *Acc. Chem. Res.*, 2019, **52**, 1575–1587.

4 S. Kumar, *Chemistry of discotic liquid crystals: From monomers to polymers*, CRC Press, 2016.

5 N. Tober, T. Rieth, M. Lehmann and H. Detert, *Chem. – A Eur. J.*, 2019, **25**, 15295–15304

6 V. Balzani, G. Bergamini and P. Ceroni, *Angew. Chemie - Int. Ed.*, 2015, **54**, 11320–11337.

7 T. Kato, J. Uchida, T. Ichikawa and T. Sakamoto, *Angew. Chem. Int. Ed.*, 2018, **57**, 4355.

8 A. Natansohn and P. Rochon, *Chem. Rev.*, 2002, **102**, 4139–4175.

9 H. M. D. Bandara and S. C. Burdette, *Chem. Soc. Rev.*, 2012, **41**, 1809–1825.

10 A. L. Leistner and Z. L. Pianowski, *European J. Org. Chem.*, 2022, e202101271.

11 G. A. Leith, C. R. Martin, A. Mathur, P. Kittikhunnatham, K. C. Park and N. B. Shustova, *Adv. Energy Mater.*, 2022, **12**, 2100441.

12 H. Sugiyama, S. Sato and K. Nagai, *Polym. Adv. Technol.*, 2022, **33**, 2113–2122.

13 B. Zhang, Y. Feng and W. Feng, *Nano-Micro Lett.*, 2022, **14**, 138.

14 I I. Dominguez-Candela, I. Zulkhairi, I. Pintre, N. F. K. Aripin, J. Lora-Garcia, V. Fombuena, M. B. Ros and A. Martinez-Felipe, *J. Mater. Chem. C*, 2022, **10**, 18200–18212.

15 M. Alaasar, *Liq. Cryst.*, 2016, **43**, 2208–2243.

16 D. A. Paterson, J. Xiang, G. Singh, R. Walker, D. M. Agra-Kooijman, A. Martínez-Felipe, M. Gao, J. M. D. Storey, S. Kumar, O. D. Lavrentovich and C. T. Imrie, *J. Am. Chem. Soc.* **2016**, *138*, 5283.

17 M. Spengler, R. Y. Dong, C. A. Michal, M. Pfletscher and M. Giese. *J. Mater. Chem. C*, 2017, **5**, 2235-2239.

18 M. Saccone, M. Spengler, M. Pfletscher, K. Kuntze, M. Virkki, C. Wölper, R. Gehrke, G. Jansen, P. Metrangolo, A. Priimagi and M. Giese. *Chem. Mater.*, 2019, **31**, 462-470.

19 M. Alaasar, X. Cai, F. Kraus, M. Giese, F. Liu and C. Tschierske, *J. Mol. Liq.*, 2022, **351**, 118597.

20 M. Li, J. Zheng, X. Wang, R. Yu, Y. Wang, Y. Qiu, X. Cheng, G. Wang, G. Chen, K. Xie and J. Tang, *Nat. Commun.*, 2022, **13**, 4912.

21 M. L. Nguyen and B.-K. Cho, *Chem. Eur. J.*, 2020, **26**, 6964-6975.

22 K. Kishikawa, S. Nakahara, Y. Nishikawa, S. Kohmoto and M. Yamamoto, *J. Am. Chem. Soc.*, 2005, **127**, 2565-2571.

23 W. Haase, D. Kilian, M. A. Athanasspoulou, D. Knawby, T. M. Swager and S. Wróbel, *Liq. Cryst.*, 2002, **29**, 133 -139

24 A. Concellón, R.-Q. Lu, K. Yoshinaga, H.-Fu Hsu and T. M. Swager, *J. Am. Chem. Soc.*, 2021, **143**, 9260−9266.

25 D. Adam, F. Closs, T. Frey, D. Funhoff, D. Haarer, P. Schuhmacher and K. Siemensmeyer, *Phys. Rev. Lett.*, 1993, **70**, 457–460.

26 D. Adam, P. Schuhmacher, J. Simmerer, L. Häussling, K. Siemensmeyer, K. H. Etzbachi, H. Ringsdorf and D. Haarer, *Nature*, 1994, **371**, 141–143.

27 O. Kasdorf, J. Vollbrecht, B. Ohms, U. Hilleringmann, H. Bock and H. S. Kitzerow, *Int. J. Energy Res.*, 2014, **38**, 452–458.

28 J.-F. Wang, Y. Kawabe, S. E. Shaheen, M. M. Morrell, G. E. Jabbour, P. A. Lee, J. Anderson, N. R. Armstrong, B. Kippelen, E. A. Mash and N. Peyghambarian, *Adv. Mater.*, 1998, **10**, 230–233.

29 A. K. Yadav, B. Pradhan, H. Ulla, S. Nath, J. De, S. K. Pal, M. N. Satyanarayan and A. S.

Achalkumar, *J. Mater. Chem. C*, 2017, **5**, 9345–9358.

30 K. Kotwica, A. S. Kostyuchenko, P. Data, T. Marszalek, L. Skorka, T. Jaroch, S. Kacka, M. Zagorska, R. Nowakowski, A. P. Monkman, A. S. Fisyuk, W. Pisula and A. Pron, *Chem. - A Eur. J.*, 2016, **22**, 11795–11806.

31 A. M. Van De Craats, N. Stutzmann, O. Bunk, M. M. Nielsen, M. Watson, K. Müllen, H. D. Chanzy, H. Sirringhaus and R. H. Friend, *Adv. Mater.*, 2003, **15**, 495–499.

32 W. Pisula, A. Menon, M. Stepputat, I. Lieberwirth, U. Kolb, A. Tracz, H. Sirringhaus, T. Pakula and K. Müllen, *Adv. Mater.*, 2005, **17**, 684–689.

33 Handbook of Liquid Crystals, 2nd ed. (Eds.: J. W. Goodby, P. J. Collings, H. Gleeson, P. Raynes, T. Kato, C. Tschierske), Non-conventional liquid crystals. Wiley-VCH, Weinheim, 2014; Volume **5**.

34 X. Zeng and G. Ungar, *J. Mater. Chem. C.*, 2020, **8**, 5389–5398.

35 Y. Cao, M. Alaasar, A. Nallapaneni, M. Salamończyk, P. Marinko, E. Gorecka, C. Tschierske, F. Liu, N. Vaupotič and C. Zhu, *Phys. Rev. Lett.*, 2020, **125**, 027801.

36 C. Dressel, F. Liu, M. Prehm, X. B. Zeng, G. Ungar and C. Tschierske, *Angew. Chem. Int. Ed.* 2014, **53**, 13115–13120.

37 C. Dressel, T. Reppe, S. Poppe, M. Prehm, H. Lu, X. Zeng, G. Ungar and C. Tschierske, *Adv. Funct. Mater.*, 2020, **30**, 2004353.

38 T. Reppe, S. Poppe, X. Cai, Y. Cao, F. Liu and C. Tschierske, *Chem. Sci*., 2020, **11**, 5902–5908.

39 M. Alaasar, A. F. Darweesh, X. Cai, Y. Cao, F. Liu and C. Tschierske, *Chem. Eur. J*., 2021, **27**, 14921–14930.

40 M. Alaasar, A. F. Darweesh, C. Anders, K. Iakoubovskii, M. Yoshio, *Mater. Adv.*, 2023, DOI: 10.1039/D3MA00841J.

41 O. Kwon, X. Cai, W. Qu, F. Liu, J. Szydlowska, E. Gorecka, M. J. Han, D. K. Yoon, S. Poppe and C. Tschierske, *Adv. Funct. Mater*., 2021, **31**, 2102271.

42 O. Kwon, X. Cai, A. Saeed, F. Liu, S. Poppe and C. Tschierske, *Chem. Commun.*, 2021, **57**, 6491–6494.

43 M. Alaasar, S. Poppe, Q. Dong, F. Liu and C. Tschierske, *Angew. Chem. Int. Ed.*, 2017, **56**, 10801-10805.

44 M. Alaasar, S. Poppe, Y. Cao, C. Chen, F. Liu, C. Zhu and C. Tschierske, *J. Mater. Chem. C*., 2020, **8**, 12902–12916.

45 M. Alaasar, M. Prehm, Y. Cao, F. Liu and C. Tschierske, *Angew. Chem. Int. Ed*., 2016, **128**, 320–324.

46 M. Alaasar, Y. Cao, Y. Liu, F. Liu and C. Tschierske, *Chem.–A Eur. J.*, 2022, **28**, e202201857.

47 Y. Cao, M. Alaasar, L. Zhang, C. Zhu, C. Tschierske and F. Liu, *J. Am. Chem. Soc.*, 2022, **144**, 6936-6945.

48 J. Matraszek, D. Pociecha, N. Vaupotič, M. Salamończyk, M. Vogrin and E. Gorecka, *Soft Matter*, 2020, **16**, 3882–3885.

49 M. Alaasar and S. Poppe, *J. Mol. Liq.*, 2022, **351**, 118613.

50 M. Alaasar, X. Cai, Y. Cao and F. Liu, *New J. Chem.*, 2022, **46**, 15871–15881.

51 T. J. Dingemans and E. T. Samulski, *Liq. Cryst.*, 2000, **27**, 131–136.

52 L. A. Madsen, T. J. Dingemans, M. Nakata and E. T. Samulski, *Phys. Rev. Lett.*, 2004, **92**, 145505.

53 B. R. Acharya, A. Primak and S. Kumar, *Phys. Rev. Lett.*, 2004, **92**, 145506.

54 F. Vita, T. Tauscher, F. Speetjens, E. T. Samulski, E. Scharrer and O. Francescangeli, *Chem. Mater.*, 2014, **26**, 4671–4674.

55 H. F. Gleeson, S. Kaur, V. Görtz, A. Belaissaoui, S. Cowling and J. W. Goodby, *ChemPhysChem*, 2014, **15**, 1251–1260.

56 V. Görtz and J. W. Goodby, *Chem. Commun.*, 2005, 3262–3264.

57 M. Nagaraj, K. Usami, Z. Zhang, V. Görtz, J. W. Goodby and H. F. Gleeson, *Liq. Cryst.*, 2014, **41**, 800–811.

58 M. Nagaraj, J. C. Jones, V. P. Panov, H. Liu, G. Portale, W. Bras and H. F. Gleeson, *Phys. Rev. E - Stat. Nonlinear, Soft Matter Phys.*, 2015, **91**, 042504.

59 A. Belaissaoui, S. J. Cowling and J. W. Goodby, *Liq. Cryst.*, 2013, **40**, 822–830.

60 N. A. Zafiropoulos, W. Lin, E. T. Samulski, T. J. Dingemans and S. J. Picken, *Liq. Cryst.*, 2009, **36**, 649–656.

61 S. W. Choi, S. Kang, Y. Takanishi, K. Ishikawa, J. Watanabe and H. Takezoe, *Chirality*, 2007, **19**, 250–254.

62 S. Kang, Y. Saito, N. Watanabe, M. Tokita, Y. Takanishi, H. Takezoe and J. Watanabe, *J. Phys. Chem. B*, 2006, **110**, 5205–5214.

63 I. H. Chiang, C. J. Long, H. C. Lin, W. T. Chuang, J. J. Lee and H. C. Lin, *ACS Appl. Mater. Interfaces*, 2014, **6**, 228–235.

64 E. Westphal, H. Gallardo, N. Sebastián, A. Eremin, M. Prehm, M. Alaasar and C. Tschierske, *J. Mater. Chem. C*, 2019, **7**, 3064–3081

65 J. Han, *J. Mater. Chem. C*, 2013, **1**, 7779–7797.

66 A. Paun, N. D. Hadade, C. C. Paraschivescu and M. Matache, *J. Mater. Chem. C*, 2016, **4**, 8596–8610.

67 S. K. Pathak, S. Nath, J. De, S. K. Pal and A. S. Achalkumar, *New J. Chem.*, 2017, **41**, 4680–4688.

68 B. G. Kim, S. Kim, J. Seo, N. K. Oh, W. C. Zin and S. Y. Park, *Chem. Commun.*, 2003, **3**, 2306–2307.

69 A. A. Vieira, E. Cavero, P. Romero, H. Gallardo, J. L. Serrano and T. Sierra, *J. Mater. Chem. C*, 2014, **2**, 7029–7038.

70 E. Westphal, M. Prehm, I. H. Bechtold, C. Tschierske and H. Gallardo, *J. Mater. Chem. C*, 2013, **1**, 8011–8022.

71 V. Gortz and J. W. Goodby, *Chem. Commun.,* 2005*,* 3262–3264.

72 D. H. Wang, Z. Shen, M. Guo, S. Z. D. Cheng, and F. W. Harris, *Macromolecules* 2007, **40**, 889–900.

73 K. Iakoubovskii and M. Yoshio, *Chem. Commun.*, 2023, **59**,7443–7446.

74 R. D. Nelson, D. R. Lide and A. A. Maryott, "Selected Values of Electric Dipole Moments for Molecules in the Gas Phase". *National Standard Reference Data Series* 10, 1967.

75 M. Alaasar, M. Prehm, S. Belau, N. Sebastián, M. Kurachkina, A. Eremin, C. Chen, F. Liu and C. Tschierske, *Chem. Eur. J*., 2019, **25**, 6362-6377.

76 M. Spengler, R. Y. Dong, C. A. Michal, W. Y. Hamad, M. J. MacLachlan and M. Giese, *Adv. Funct. Mater.*, 2018, **28**, 1800207.